Accepted Manuscript

High-efficiency adsorption for acid dyes over $CeO_2 \cdot xH_2O$ synthesized by a facile method

Hui Wang, Yunchao Zhong, Huimin Yu, Paolo Aprea, Shiyou Hao

PII: S0925-8388(18)33902-1

DOI: 10.1016/j.jallcom.2018.10.228

Reference: JALCOM 48046

To appear in: *Journal of Alloys and Compounds*

Received Date: 4 September 2018

Revised Date: 15 October 2018

Accepted Date: 18 October 2018

Please cite this article as: H. Wang, Y. Zhong, H. Yu, P. Aprea, S. Hao, High-efficiency adsorption for acid dyes over $CeO_2 \cdot xH_2O$ synthesized by a facile method, *Journal of Alloys and Compounds* (2018), doi: https://doi.org/10.1016/j.jallcom.2018.10.228.

This is a PDF file of an unedited manuscript that has been accepted for publication. As a service to our customers we are providing this early version of the manuscript. The manuscript will undergo copyediting, typesetting, and review of the resulting proof before it is published in its final form. Please note that during the production process errors may be discovered which could affect the content, and all legal disclaimers that apply to the journal pertain.

ACCEPTED MANUSCRIPT

High-Efficiency Adsorption for Acid Dyes over $CeO_2 \cdot xH_2O$ Synthesized by a Facile Method

Hui Wang [b], Yunchao Zhong[a], Huimin Yu[a], Paolo Aprea[c], Shiyou Hao [a,*]

[a]Xingzhi College, Zhejiang Normal University, 321004 Jinhua，P. R. of China

[b]College of Chemistry and Life Sciences, Zhejiang Normal University, 321004 Jinhua，P. R. of China

[c]Department of Chemical, Materials and Production Engineering, University Federico II, P.le V. Tecchio 80, 80125, Naples, Italy

*Corresponding author：

Tel. / Fax: +86 579 82287468, E-mail: sky54@zjnu.cn (Shiyou Hao)

ACCEPTED MANUSCRIPT

Abstract

In this study, $CeO_2 \cdot xH_2O$ with high-efficiency adsorption for acid dyes was synthesized via a facile method. Effect of temperature, pH and aging time in synthesis on the removal of acid red 14 (AR14) was investigated. It was found that the $CeO_2 \cdot xH_2O$ prepared at 25 ^{O}C, pH of 4.5, and aged for 6 h is suitable for adsorption of AR14 and acid orange 7 (AO7) because of a large number of hydroxyl groups, NH_4^+ and oxygen vacancies in the resulting sample. The unary adsorption isotherm of AR14 on the optimized $CeO_2 \cdot xH_2O$ adsorbent is well described by the Langmuir model, with an estimated adsorption capacity of 540 mg/g, which is a much higher value than those reported in literature. 100% of AR14 or 33% of AO7 in 40 ml of 250 mg/l aqueous solution can be removed by 0.02 g of the optimized $CeO_2 \cdot xH_2O$ adsorbent. The $CeO_2 \cdot xH_2O$ adsorbent also shows a good stability through several adsorption-regeneration cycles. Based on these excellent properties, the application in the removal of acid dyes from wastewater is anticipated. Furthermore, a novel adsorption mechanism was proposed based on the interaction between sulfonic groups ($-SO_3^-$) in acid dyes and protonated hydroxyl groups ($-OH_2^+$), ammonium radicals (NH_4^+), and oxygen vacancies ($V_O^{\bullet\bullet}$) on the surface of the optimized $CeO_2 \cdot xH_2O$ sample.

Keywords: $CeO_2 \cdot xH_2O$; Synthesis; Adsorption; Acid dyes; Adsorption mechanism

1. Introduction

It is well known that environmental pollution is identified as one of the largest problems of modern society [1]. Synthetic dyes, very hazardous pollutants, represent a relatively large group of organic chemicals that are found in practically all over the world. The discharge of dyes into water bodies and/or ground water is a serious problem in environmental protection and wastewater treatment. Dyes and their degradation products are mutagenic, teratogenic and carcinogenic, which are certainly harmful to aquatic organisms and human health [2]. With increasing industrialization, acid dyes such as AR14 and AO7 are commonly detected in industrial effluents. Therefore, industrial effluents containing high levels of acid dyes must be treated before being released into the environment.

To remove acid dyes from wastewater, a number of techniques, such as ion exchange, precipitation, adsorption, chemical oxidation, photocatalysis, etc., have been employed [3-7]. Among these methods, adsorption is an attractive and favorable technique due to its simplicity of operation, sludge free and wide application range [8]. Furthermore, the adsorbents can be recycled via desorption, resulting in a low cost in practical application. Usually, activated carbon is used as an adsorbent to remove acid dyes from wastewater due to its high-efficiency adsorption [9]. However, the high cost of activated carbon restricts its practical application. Consequently, low-cost adsorbents, such as clay minerals [10], fly ash [11], natural plant waste [12], have attracted much attention, but low adsorption capacities and consequent large adsorbent dosage limit their comprehensive use. In order to obtain adsorbents with low-cost and high adsorption capacity, considerable efforts have been made in recent years.

Using light rare earth hydroxides, such as $La(OH)_3$, $Pr(OH)_3$, $Nd(OH)_3$, as adsorbents [13],

many dyes can be efficiently removed from water mainly due to the role of hydroxyl groups. Generally, hydrogen bonds and electrostatic forces between hydroxyl groups and dye molecules can be formed, which account for the removal of dyes over the earth hydroxides [14]. For example, Wang et al. developed a facile hydrothermal approach for the synthesis of porous nanowires of layered hydroxide lanthanum acetate (LHL-acetate) and used the prepared material as adsorbent to remove Congo red in water solution. The results showed that 15 ml of 100 mg/l Congo red solution can be changed colorless in 15 min after adsorption by 0.01 g of LHL-acetate porous nanowires, which demonstrate an estimated capacity for Congo red of 270 mg/g [15]. Zhai and co-workers reported the electrochemical synthesis of porous $Pr(OH)_3$ nanobelt arrays, nanowire arrays, nanowire bundles, and nanowires and their applications as dye absorbents in water treatment. The results illustrated that the amount of Congo red adsorbed onto $Pr(OH)_3$ nanowires can reach 500 mg/g in 120 min [14]. Qu and co-workers prepared porous $Nd(OH)_3$ nanobelts and found that 0.02 g of the as-prepared sample can remove 99.1% of Congo red contained in 50 ml of 100 mg/l water solution in 30 min and its adsorption capacity for Congo red reached up to 250 mg/g [16]. As a member of light rare earth, Ce has similar properties to those of La, Pr, Nd. Therefore, it can be inferred that cerium hydroxide, mainly represented by $Ce(OH)_4$ because of the easy oxidation of $Ce(OH)_3$ by oxygen in the air [17], may be an efficient adsorbent for removal of dyes from wastewater. Generally, pure $Ce(OH)_4$ is difficult to obtain because it easily loses some water, becoming $CeO_2 \cdot xH_2O$, especially when it is subjected to relative high temperature [18], resulting in the decrease of hydroxyl content. Presumably, a higher hydroxyl content in $CeO_2 \cdot xH_2O$ will lead to a good adsorption efficiency.

In this paper, with the aim to obtain $CeO_2 \cdot xH_2O$ samples with high hydroxyl content and hence high-efficiency adsorption for acid dyes *via* a simple method, we report a facile synthesis of $CeO_2 \cdot xH_2O$ with high loading of hydroxyl groups starting from $Ce(NO_3)_3 \cdot 6H_2O$ and ammonia as reactants *via* adjusting synthesis temperature, pH value, and aging time. Using the as-prepared samples as adsorbents for the removal of AR14 containing water solution, it is found that AR14 can be easily removed from water and the adsorption capacity of the resulted $CeO_2 \cdot xH_2O$ can reach up to 540 mg/g, much higher than those reported in literature. Furthermore, the role of amino groups and oxygen vacancies in the adsorption and a novel mechanism of acid dyes adsorption over $CeO_2 \cdot xH_2O$ were proposed.

2. Experimental

2.1 Chemicals and synthesis

Cerium(III) nitrate hexahydrate ($Ce(NO_3)_3 \cdot 6H_2O$), ammonium hydroxide ($NH_3 \cdot H_2O$, 27%), sodium hydroxide (NaOH), absolute ethanol, and 37% fuming hydrochloric acid were purchased from Sinopharm Chemical Reagent Co. All the chemical reagents were used without further purification. Deionized water with a resistivity larger than 18.2 MΩ was obtained from Millipore Milli-Q® ultrapure water purification systems. 0.2 M of HCl solution was prepared from the 37% fuming hydrochloric acid. 2 mM solution of dyes were obtained by dissolved AR14 and AO7 (Sigma-Aldrich) in deionized water at room temperature. The pH values of all the solutions containing AR14 or AO7 used for the adsorption experiments were adjusted to the desired ones using 0.2 M HCl or 0.2 M NaOH solution.

A typical synthesis of $CeO_2 \cdot xH_2O$ can be described as follows: 4.34 g of $Ce(NO_3)_3 \cdot 6H_2O$ was dissolved into 50 ml of deionized water at room temperature under stirring. After the

solution became clear, a certain amount of ammonium hydroxide ($NH_3 \cdot H_2O$, 27%) was added into the solution to adjust solution pH to the desired value (6.5, 7.7, 8.5, 9.5, 10.5) at different temperature (0, 25, 40, 55 ℃). At this point, a light-brown precipitate was formed in the solution. Afterwards, the precipitate was aged by keeping it static at room temperature for different times (1, 6, 12, 24 h). The solid was then recovered by filtration, washed with water and ethanol for three times, and dried at 80 ℃, respectively.

2.2 Characterization

The X-ray diffraction (XRD) patterns were collected on a Philips PW3040/60 powder diffractometer using CuKα radiation (λ = 0.154 nm). The FT-IR spectra were recorded by a Nicole Nexus 670 spectrometer with a resolution of 4 cm^{-1} using the KBr pellet method. The thermogravimetric analysis (TGA) was performed on a NETZSCH STA 449C thermogravimetric analyzer with a temperature ramp of 10 ℃/min in air. X-ray photoelectron spectroscopy (XPS) measurement was carried out on a RBO upgraded PHI-5000 C ESCA system (Perkin Elmer) using monochromated Al Kα X-rays (E=1486.6 eV) as a radiation at 250 W. All binding energies were calibrated using carbon (C_{1S} = 284.6 eV) as a reference.

2.3 Adsorption experiment

A certain amount of as-prepared $CeO_2 \cdot xH_2O$ was added to a certain volume of AR 14 solution (250 mg/l) under stirring. At given time intervals, a small amount of suspension was withdrawn and centrifuged to remove the adsorbent. The residual AR14 levels in the filtrates were then analyzed by recording the variations of the absorbance at 516 nm with a UV-vis spectrophotometer (Evolution 500LC). The removal efficiency of AR14 by the adsorbent was represented by C/C_0, where C_0 (mg/l) is the initial concentration of AR14 and C (mg/l) is the

concentration of AR14 at time *t* (min).

Especially, effects of sample preparation conditions, such as temperature, pH value, aging time, on the removal efficiency of AR14 were studied in detail. Based on the adsorbent synthesized *via* the optimal route, adsorption kinetics, effect of the aqueous solution pH value on the removal efficiency, adsorption equilibrium, etc. were discussed.

2.3.1 Adsorption kinetics

0.02 g of the adsorbent was suspended in 40 ml of 250 mg/l AR14 solution with an inintial pH value of 5.23, under vigorous stirring at 25 ^{0}C for different times. The mixture was then quickly filtered to remove the adsorbent and the solution was analyzed by the UV-vis spectrophotometer.

2.3.2 Effect of the adsorption solution pH value on the removal efficiency of AR14

0.02 g of the prepared adsorbent was suspended in 20 ml of 250 mg/l solution containing AR14 at different pH values ranging from 3.5 to 6.5. The mixture was stirred for 30 min, then centrifuged at 10000 rpm for 10 min, and finally separated into liquid and solid phases. The collected solution was analyzed by UV-vis spectrophotometer to determine the concentration of AR14.

2.3.3 Adsorption equilibrium

The adsorption isotherm data were calculated by the following equation:

$$q_e = \frac{(C_0 - C_e)V}{W} \quad (1)$$

where q_e (mg/g) is the adsorbed amount of AR14 on the adsorbent, C_0 (mg/l) is the initial concentration of AR14, C_e (mg/l) is the equilibrium concentration of AR14, V (l) is the volume of the used solution containing AR14, and W (g) is the weight of the used adsorbent. The

adsorption isotherm data of AR14 on the $CeO_2 \cdot xH_2O$ adsorbent were determined using 0.02 g of $CeO_2 \cdot xH_2O$ suspended in 40 ml of the solutions containing AR14 with concentrations ranging from 100.4 to 753 mg/l for an adsorption time of 30 min under vigorous stirring at the optimized pH and 25 ^{0}C (stabilized by water bath).

The Langmuir isotherm model was used to describe the adsorption isotherm:

$$q_e = \frac{Q_{\max} K_L C_e}{1 + K_L C_e} \quad (2)$$

where q_e (mg/g) is the adsorbed amount of AR14 on the adsorbent, Q_{max} (mg/g) is the saturation adsorption capacity, C_e (mg/l) is the equilibrium concentration of AR14, and K_L is the equilibrium adsorption constant.

2.3. 4 Adsorbent regeneration

The regeneration of the used adsorbent was carried out as follows. Typically, an adsorption run was performed suspending 0.02 g of $CeO_2 \cdot xH_2O$ in 40 ml of 250 mg/l AR14 solution. After that, the exhausted sample was treated with 10 ml of 2 M NaOH solution under vigorous stirring at 50 °C for 1 h, followed by washing with deionized water for several times and drying at 80 °C for 2 h. The regenerated adsorbent was then used for the next run. Six successive adsorption-regeneration cycles were performed to check the reusability of the developed adsorbent for capturing AR14.

3. Results and discussion

Effect of reaction temperature on the removal of AR14 at an initial pH value of 5.32 is shown in Fig. 1. It is clear from Fig. 1 that the removal efficiency of AR 14 over $CeO_2 \cdot xH_2O$ decrease gradually with increasing reaction temperature. A possible explanation can come from the analysis of the reactions occurring during the $CeO_2 \cdot xH_2O$ synthesis process. At first,

ammonia ionize to form ammonium ion and hydroxyl group, as presented by equation 3. Afterwards, Ce^{3+} interact with OH^- to produce $Ce(OH)_3$ precipitate (see equation 4), which is easily oxidized by dissolved oxygen to form $Ce(OH)_4$ (see equation 5). Finally, part of water is lost from $Ce(OH)_4$ and $CeO_2 \cdot xH_2O$ is obtained, as shown by equation 6. From a thermodynamic point of view, lowering temperature is beneficial to exothermic reactions. According to the calculation based on the standard molar enthalpy of formation ($\Delta_f H_m^\theta$), the reaction enthalpy ($\Delta_r H_m^\theta$, $\Delta_r H_m^\theta = \Delta_f H_m^\theta(NH_4^+) + \Delta_f H_m^\theta(OH^-) - \Delta_f H_m^\theta(NH_3) - \Delta_f H_m^\theta(H_2O)$) = -30.56 kJ/mol) of equation 3 is a negative value, indicating that the ionization of ammonia is exothermic. Therefore, hydroxyl groups are easy to be produced at lower temperatures, and Ce^{3+} can be easily captured by OH^- to produce $Ce(OH)_3$. From the principle of colloid adsorption, it can be inferred that hydroxyl groups are preferentially adsorbed by $Ce(OH)_3$ and $Ce(OH)_4$. Consequently, the content of hydroxyl groups in the resulted sample is much high and thus the removal efficiency of AR14 over the prepared adsorbent is enhanced due to the interaction between hydroxyl groups and sulfonic acid groups in AR14 in the acid system [14].

$$NH_3 + H_2O = NH_4^+ + OH^- \quad (3)$$

$$Ce^{3+} + 3OH^- = Ce(OH)_3 \quad (4)$$

$$4Ce(OH)_3 + O_2 + 2H_2O = 4Ce(OH)_4 \quad (5)$$

$$Ce(OH)_4 - (2-x)\,H_2O = CeO_2 \cdot xH_2O \ (x<2) \quad (6)$$

In order to prove the above hypothesis, we used in situ FT-IR to compare the relative hydroxyl content for the samples synthesized at different temperatures. The concentration of hydroxyl groups can be measured from the integral area of Ce-OH band after the complete

removal of physisorbed water for the different samples, and the results are shown in Fig. 2. Generally, the broad adsorption at 2800-3800 cm^{-1} is mainly attributed to the stretching OH (ν_{O-H}) contributed by both water and hydroxyl groups [19]. However, the physisorbed water may be mostly removed because all the samples were evacuated under vacuum at 110 ^{0}C for 4 h. Therefore, the band at 2800-3800 cm^{-1} is ascribed to the vibration of hydroxyl groups. As it can be seen from Fig. 2, the concentration of hydroxyl groups increases gradually with decreasing reaction temperature, in good agreement with our assumption.

As we known, the hydroxyl concentration during the synthesis is related to the pH value, resulting in formation of products with different properties. Therefore, the reaction pH value plays an important role during the removal of AR14 from wastewater. Effect of reaction pH on the removal of AR14 is illustrated in Fig. 3. From Fig. 3, it is easily seen that the removal efficiencies of AR14 over the $CeO_2 \cdot xH_2O$ prepared at pH of 7.7 and 8.5 are higher than those of adsorbents synthesized at pH of 9.5 and 10.5, and the adsorption rate of $CeO_2 \cdot xH_2O$ prepared at pH of 8.5 is faster than those of other samples. From the synthesis procedure, it can be calculated that the concentration of Ce^{3+} in the synthesis batch is 0.2 M. When the initial reaction pH value is 7.7, pale yellow $Ce(OH)_3$ precipitate is produced because the concentration product (J, $2\times10^{-19.9}$) of Ce^{3+} and $(OH^-)^3$ is higher than the concentration product constant of $Ce(OH)_3$ (K_{sp}^{θ}, 1.6×10^{-20}). When the reaction pH value is increased to 8.5, a large amount of precipitate is immediately formed due to the higher concentration product ($1.6\times10^{-17.5}$). At this point, the concentration of Ce^{3+} is decreased to $1.6\times10^{-3.5}$, implying that Ce^{3+} is almost precipitate completely. Therefore, the adsorption capability of NH_4^+ over the $Ce(OH)_3$ can be improved greatly due to the selective adsorption properties of colloids, which

enhance the interaction between the adsorbent and AR14 *via* the electrostatic attraction, resulting in a very fast adsorption rate. It is easy to find from Fig. 3 that all the adsorption processes are very fast at initial period due to a large number of hydroxyl groups on the surface of adsorbents, which can be proved by the results of Fig. 4. However, there is a slight decrease in the concentration of dye using the samples synthesized at pH of 7.7, 9.5, and 10.5 as adsorbents because some of adsorption sites are occupied by AR14 after initial adsorption. It can be concluded from Fig. 4 that the concentration of hydroxyl groups and ammonium ions of the sample prepared at pH of 8.5 is higher than those of samples synthesized at pH of 7.7, 9.5, and 10.5, resulting in more adsorption sites. Consequently, the concentration of AR 14 was decreased to almost zero at the initial stage of adsorption.

In order to identify the presence of NH_4^+ in the $CeO_2 \cdot xH_2O$ synthesized at pH of 8.5, IR-FT was performed and the results are presented in Fig. 4a. As previously stated, the bands observed in the 2800-3800 cm^{-1} interval are due to hydroxyl groups and water. Moreover, the peaks present around 1324 and 1467 cm^{-1} are ascribed to the -N-H bending vibration modes [20, 21]. The peak at 1043 cm^{-1} corresponds to the bending vibration of hydroxyl groups of metal oxides (M-OH) [22]. The O-H bending vibration of interstitial water molecule appears at 1623 cm^{-1} [23]. The band at 1384 cm^{-1} is due to the stretching vibration of the redundant NO_3^- on the surface of the prepared samples [24]. It can be seen from Fig. 4a that the intensity of bands at 1324 and 1467 cm^{-1} for the sample synthesized at pH of 8.5 is much higher than those of samples prepared at pH of 7.7 and 9.5, and that the hydroxyl groups in the sample prepared at pH of 8.5 are more abundant due to the higher peak intensity at 1043 and 1623 cm^{-1}, which results in a higher adsorption efficiency. When the reaction pH value is increased to 9.5, some

hydroxyl groups in the resulted sample can be deprotonated to form oxygen anions [25] and thus the removal efficiency of AR14 decrease because the content of hydroxyl groups and NH_4^+ is lower, which , again, can be verified by the results of FT-IR. In order to testify the adsorption of AR 14 over the $CeO_2 \cdot xH_2O$ sample, FT-IR was also carried out for the sample synthesized at pH of 8.5 after adsorption and the result is presented in Fig. 4b. It is evident from Fig. 4b that AR14 was really adsorbed on the $CeO_2 \cdot xH_2O$ sample because the characteristic peaks of AR14 are detected after adsorption. For example, the peak around 1473 cm^{-1} is ascribed to the azo bond (–N=N–), the 1504 cm^{-1} band is due to benzene ring vibration, and the vibration of sulfonic group (–SO_3H) is present at about 1277 cm^{-1} [20].

In order to further prove the role of NH_4^+ in the removal of AR14, 2 M NaOH aqueous solution was used as precipitant to synthesize $CeO_2 \cdot xH_2O$ and the reaction pH value was also adjusted to 8.5. The removal efficiency of AR14 over the $CeO_2 \cdot xH_2O$ synthesized by NaOH and $NH_3 \cdot H_2O$ is shown in Fig. 5. It can be found from Fig. 5 that the adsorption rate of $CeO_2 \cdot xH_2O$ synthesized by $NH_3 \cdot H_2O$ is much higher than that of adsorbent prepared by NaOH. AR14 can be removed completely by the $CeO_2 \cdot xH_2O$ in 2 min when $NH_3 \cdot H_2O$ was used as precipitant, but only 60% of AR14 was adsorbed on the sample synthesized by NaOH at this time, implying the contribution of NH_4^+ in the removal of AR14 over the resulted adsorbent. From Fig. 14, it is clear that the electrostatic attraction can be formed between NH_4^+ and -SO_3^- groups present in acid dyes, which improve the adsorption efficiency of the sample synthesized by using $NH_3 \cdot H_2O$ as precipitant, especially at the initial period of adsorption.

From the previous reports, it can be found that aging time in synthesis is also an important factor affecting the target samples properties, such as morphology, particle size, and specific

surface area [26, 27]. Effect of aging time on the removal of AR14 is illustrated in Fig. 6, and the results show that the removal efficiency of AR14 increases with increasing aging time from 1-6 h, and then decreases with further increasing aging time. This can be due to the fact that a large amount of hydroxyl groups cannot be generated in a short time because ionization of ammonium is a reversible reaction (see equation 3). Generally, the nucleation and growth of $Ce(OH)_3$ and $Ce(OH)_4$ also take some time. On the contrary, a too long aging time will lead to the increase of grain size and the decrease of specific surface [28], resulting in lower adsorption efficiency. Furthermore, more water molecules may be lost from the $CeO_2 \cdot xH_2O$ when the aging time is too long, leading to fewer hydroxyl groups in the resulted samples, which will decrease the quantity of NH_4^+ in the $CeO_2 \cdot xH_2O$ sample due to the decreased number of negative group (OH^-). Consequently, the best aging time for the adsorption must be determined. It can be seen from Fig. 6 that the optimum aging time for AR14 adsorption over the $CeO_2 \cdot xH_2O$ is 6 h under our experimental conditions.

In order to testify the above deduction, FT-IR spectra of $CeO_2 \cdot xH_2O$ prepared at different aging time were obtained and the results are presented in Fig. 7. It can be seen from Fig. 7 that the intensity of bands at 1043 and 1623 cm^{-1} for the sample aged for 6 h is much higher than that of samples aged for 1 and 24 h, respectively, indicating that the sample aged for 6 h has higher loading of hydroxyl groups compared with other samples. From the comparative analysis of peak intensity for 1324 and 1467 cm^{-1}, it can be inferred that the content of NH_4^+ in the $CeO_2 \cdot xH_2O$ aged for 6 h is also higher than that of samples aged for 1 and 24 h. Consequently, the interaction between $CeO_2 \cdot xH_2O$ aged for 6 h and AR14 is more effectively due to the stronger electrostatic attraction between $-OH_2^+$ (NH_4^+) and $-SO_3^{2-}$.

From the above discussion, it can be concluded that $CeO_2 \cdot xH_2O$ synthesized at 25 ^{O}C and pH of 8.5 and aged for 6 h, referred to the target $CeO_2 \cdot xH_2O$, will possess a good adsorption for AR14 aqueous solution. According to this assumption, the target $CeO_2 \cdot xH_2O$ was synthesized. Fig. 8 shows the powder X-ray diffraction (XRD) patterns of the target $CeO_2 \cdot xH_2O$ and standard CeO_2. It can be easily seen from Fig. 8 that the diffraction peaks of target $CeO_2 \cdot xH_2O$ are consistent with the JCPDS file of CeO_2 (JCPDS no. 34-0394), but the corresponding peak intensity is much weaker than that of standard CeO_2, which can indicate a crystal structure similar to that of $Ce(OH)_4$, as previously reported in literature [29]. In order to identify the structure composition of the target $CeO_2 \cdot xH_2O$, the weight loss (TGA) and differential thermal analysis (DTA) were performed, and the results are presented in Fig. 9. The DTA plot shows two peaks (at 83 °C and 338 °C) which indicate the presence of two different endothermic events. Such events can be correlated to the thermal decomposition of the sample: the TGA plot shows two main weight loss regions (see Fig. 8), mainly due to the loss of the adsorbed water at a temperature of about 82 °C and the decomposition of amino groups [30] and cerium hydroxides in the temperature range of 250-800 °C. The total weight loss of the target $CeO_2 \cdot xH_2O$ turned out to be of about 19.4%.

Ce3d XPS spectra of the target $CeO_2 \cdot xH_2O$ can be assigned to be $3d_{3/2}$ spin-orbit states (labeled u) and $3d_{5/2}$ states (labeled v), as presented in Fig. 10a. The band doublets u'''/v''', u''/v'', and u/v represent the chemical state of Ce^{4+} ions, while u'/v' and u_0/v_0 doublets are due to photoemission from Ce^{3+} ions. From the result of Ce3d XPS spectra, we can conclude that oxygen vacancies can be produced because Ce^{4+} can be replaced by Ce^{3+}, a lower valence state ion, according to the following equation:

$$CeO_2 \rightarrow Ce_{1-x}(\mathrm{IV})\cdot Ce_x\cdot(\mathrm{III})\cdot O_{2-x/2}\cdot(x/2)V_O^{\bullet\bullet}+(x/4)O_2 \quad (7)$$

O1s XPS spectra of the target $CeO_2\cdot xH_2O$ are shown in Fig. 10b. The O1s spectra can be resolved to three peaks located at 530.0, 531.6 and 532.8 eV, assigned to O_2, OH^- and H_2O groups, respectively [31]. It is obvious that the target sample contains much water and hydroxyl groups, in good agreement with the result of TGA.

The pH of the solution containing AR14 may affect the surface charge of the free surface hydroxyl groups [32] as well as the degree of ionization and hydrolysis of the species present in the solution. Therefore, the pH of the solution plays an important role in the adsorption of AR14 from solution. Fig. 11 shows the effects of the pH in the solution on the removal efficiency. It can be found that the removal efficiency of AR14 increases sharply with decreasing the pH value in the adsorption solution from 6.5 to 4.5 and then increase gradually with further decreasing the pH value. This may be related to the fact that the hydroxyl groups on the surface of the target $CeO_2\cdot xH_2O$ are protonated rapidly when the pH value of adsorption system decrease from 6.5 to 4.5 and most of hydroxyl groups interact with proton when the pH value is below 6.5. From Fig. 11, it can be observed that the removal efficiency of AR14 at pH of 4.5 (98.8%) is close to that at pH of 3.5 (99.6%). In sight of practical applications, the next adsorption experiments have been performed at pH value of 4.5.

The adsorption kinetics is one of the important characteristics that define the adsorption efficiency. Fig. 12a shows the uptake of AR14 in the target $CeO_2\cdot xH_2O$, which is very fast because 99% of AR14 can be removed in 5 min and the adsorption capacity of 30 min is almost not improved, indicating the uptake reaches the equilibrium within 30 min and an adsorption time of 30 min should be enough to obtain their adsorption isotherms. This is due to

the fact that the target $CeO_2 \cdot xH_2O$ has a large number of hydroxyl groups and ammonium radicals, shown in Fig. 2 and 4a, which enhance the interaction with AR14. Furthermore, oxygen vacancies, positively charged position, can combine with $-SO_3^-$ in AR14 *via* electrostatic interaction, which also improve the adsorptive rate of AR14. Moreover, it is obvious from Fig. 12b that the uptakes can be well described by the pseudo-second-order model as follows [33]:

$$\frac{t}{q_t} = \frac{1}{kq_e^2} + \frac{t}{q_e} \qquad (7)$$

The adsorption isotherm of AR14 on the target $CeO_2 \cdot xH_2O$ at room temperature is shown in Fig. 13. The plot shows a sharp increase in the adsorbed amount at low AR14 concentration, indicating that the removal efficiency is greatly high due to the high adsorption potential of the prepared adsorbent to AR14. Among the three models (Langmuir, Temkin and Freundlich) taken into account to describe the adsorption data, the Langmuir equation turned out to be the best over the full range of concentrations, as shown in Fig. 13. The saturation adsorption capacity estimated from the model is 540 mg/g, much higher than 435 mg/g on nano-polyaniline and Baker's yeast [34], 370 mg/g on amine functionalized magnetic carbon nanotube [35], 312.5 mg/g on amine functionalized itania/silica nano-hybrid [36], 217.39 mg/g on acid treated okara [37], 64.23 mg/g on NiO flowerlike architectures [38], and 196.08 mg/g on LDH/MWCNTs nanohybrid [39]. The larger saturation adsorption capacity of AR14 is ascribed to the high loading of hydroxyl groups, abundant NH_4^+ and oxygen vacancies in the target $CeO_2 \cdot xH_2O$.

The reusability of an adsorbent is crucial in practical applications. The results on 6 adsorption-regeneration cycles of AR14 on the target $CeO_2 \cdot xH_2O$ shows that the removal

efficiency is still above 96% after 6 adsorption-regeneration cycles, indicating that NaOH solution is an effective desorption effluent and the synthesized $CeO_2 \cdot xH_2O$ adsorbent is rather reusable.

We also found that the target $CeO_2 \cdot xH_2O$ has a good adsorptive efficiency for acid orange 7 (AO7) under the same experimental conditions of AR14. It can be seen from the adsorption results that the adsorption capacity of AO7 over the target $CeO_2 \cdot xH_2O$ is 164 mg/g, much higher than 22 mg/g on ceria hollow sphere [40], and 63 mg/g on ceria nanoparticles [41]. However, the adsorption capacity of AO7 over the target $CeO_2 \cdot xH_2O$ is lower than that of AR14. The reason may be that the numbers of $-SO_3^-$ in AR14 are higher than those in AO7. Based on the above analysis, the possible adsorption mechanism may be described as follows: hydroxyl groups on the surface of adsorbent are protonated to form $-OH_2^+$ in the acid system and then $-OH_2^+$ interact with the $-SO_3^-$ groups present in acid dyes by electrostatic attraction. Furthermore, NH_4^+ and oxygen vacancies on the surface of adsorbent can also capture $-SO_3^-$ by electrostatic interaction. Therefore, the possible adsorption mechanism of acid dyes over the target $CeO_2 \cdot xH_2O$ can be illustrated by the schematic diagram, as shown in Fig. 14.

4. Conclusion

$CeO_2 \cdot xH_2O$ with high loading of hydroxyl groups was successfully synthesized *via* adjusting synthesis temperature, pH value and aging time. It was found that the resulting sample has an elevated number of NH_4^+, hydroxyl groups, and oxygen vacancies on its surface. For this reason, the prepared $CeO_2 \cdot xH_2O$ possesses an excellent adsorption efficiency for AR14 compared with other adsorbents reported in literature. Moreover, $CeO_2 \cdot xH_2O$ synthesized in this study also has a good removal efficiency for AO7. Therefore, the optimized synthetic

$CeO_2 \cdot xH_2O$ is a promising candidate as highly-efficient adsorbent for the removal of acid dyes from wastewater.

Acknowledgment

The financial support by the National Natural Science Foundation of China (21876158) and the Natural Science Foundation of Zhejiang Province, China (LY14B070006) are gratefully acknowledged.

References

[1] Gupta, V. K.; Suhas. Application of low-cost adsorbents for dye removal-a review. *J. Environ. Manage.* **2009**, 90, 2313-2342.

[2] Chakraborty, S.; Basak, B.; Dutta, S.; Bhunia, B.; Dey, A. Decolorization and biodegradation of congo red dye by a novel white rot fungus Alternaria alternata CMERI F6. *Bioresour. Technol.* **2013**, 147, 662-666.

[3] Magdalena, G. Use of ion exchangers, ion exchange membranes, polymeric sorbents and biopolymers in removal of acid and reactive dyes from aqueous solutions. Przem. Chem. **2013**, 92, 469-478.

[4] Cerboneschi, M.; Corsi, M.; Bianchini, R.; Bonanni, M.; Tegli, S. Decolorization of acid and basic dyes: understanding the metabolic degradation and cell-induced adsorption/precipitation by Escherichia coli. *Appl. Microbiol. Biotechnol.* **2015**, 99, 8235-8245.

[5] Li, C. P.; Zhou, H.; Wang, S.; Yuan, H. H.; Zhang, S. Z.; Du, M. A nanoporous Ag(I)

coordination polymer for selective adsorption of carcinogenic dye Acid Red 26. *Chem. Commun.* **2017**, 53, 4767-4770.

[6] Wang, X.; Gu, X.; Zhou, X.; Wang, W.; Lin, D. Treatment of wastewater containing acid rose red dye by biologically aerated filter after chemical oxidation. *Environ. Technol.* **2007**, 28, 831-839.

[7] Zang, C.; Zhang, X.; Hu, S.; Chen, F. The role of exposed facets in the Fenton-like reactivity of CeO_2 nanocrystal to the orange II. *Appl. Catal. B: Environ.* **2017**, 216, 106-113.

[8] Wang, M. X.; Zhang, Q. L.; Yao, S. J. A novel biosorbent formed of marine-derived Penicillium janthinellum mycelial pellets for removing dyes from dye-containing wastewater. *Chem. Eng. J.* **2015**, 259, 837-844.

[9] Subramani, S. E.; Kumaresan, D.; Thinakaran, N. Application of activated carbon derived from waste delonix regia seed pods for the adsorption of acid dyes: kinetic and equilibrium studies. *Desalin. Water Treat.* **2016**, 57, 7322-7333.

[10] Elsherbiny, A. S. Adsorption kinetics and mechanism of acid dye onto montmorillonite from aqueous solutions: stopped-flow measurements. *Appl. Clay Sci.* **2013**, 83-84, 56-62.

[11] Pura, S.; Atun, G. Adsorptive removal of acid blue 113 and tartrazine by fly ash from single and binary dye solutions. *Sep. Sci. Technol.* **2009**, 44, 75-101.

[12] Lee, L. Y.; Gan, S. Y.; Tan, M. S. Y.; Lim, S. S.; Lee, X. J.; Lam, Y. F. Effective removal of acid blue 113 dye using overripe cucumis sativus peel as an eco-friendly biosorbent from agricultural residue. *J. Clean. P.* **2016**, 113, 194-203.

[13] Lu, X. H.; Zheng, D. Z.; Xu, M.; Huang, Y. Y.; Xie, S. L.; Liu, Z. Q.; Liang, C. L.; Liu, P.;

Tong, Y. X. General electrochemical assembling to porous nanowires with high adaptability to water treatment. *CrystEngComm* **2011**, 13, 2451-2456.

[14] Zhai, T.; Xie, S. L.; Lu, X. H.; Xiang, L.; Yu, M.; Li, W.; Liang, C. L.; Mo, C. H.; Zeng, F.; Luan, T. G.; Tong, Y. X. Porous $Pr(OH)_3$ nanostructures as high-efficiency adsorbents for dye removal. *Langmuir* **2012**, 28, 11078-11085.

[15] Wang, P. P.; Bai, B.; Hu, S.; Zhuang, J.; Wang, X. Family of multifunctional layered-lanthanum crystalline nanowires with hierarchical pores: hydrothermal synthesis and applications. *J. Am. Chem. Soc.* **2009**, 131, 16953-16960.

[16] Qu, J. X.; Zheng, D. Z.; Lu, X. H.; Shi, J. Y.; Lan, C. Y. Electrochemical assembling of aligned porous $Nd(OH)_3$ nanobelts with high performance in water treatment. *Inorg. Chem. Commun.* **2010**, 13, 1425-1428.

[17] Tang, C.; Bando, Y.; Liu, B.; Golberg, D. Cerium oxide nanotubes prepared from cerium hydroxide nanotubes. *Adv. Mater.* **2005**, 17, 3005-3009.

[18] Bourja, L.; Bakiz, B.; Benlhachemi, A.; Ezahri, M.; Villain, S.; Favotto, C.; Valmalette, J. C.; Gavarri, J. R. Structural modifications of nanostructured ceria $CeO_2 \cdot xH_2O$ during dehydration process. *Powder Technol.* **2012**, 215-216, 66-71.

[19] Pan, D. H.; Yuan, P.; Zhao, L. Z.; Liu, N.; Zhou, L.; Wei, G. F.; Zhang, J.; Ling, Y. C.; Fan, Y.; Wei, B. Y.; Liu, H. Y.; Yu, C. Z.; Bao, X. J. New understanding and simple approach to synthesize highly hydrothermally stable and ordered mesoporous materials. *Chem. Mater.* **2009**, 21, 5413-5425.

[20] Hao, S. Y.; Hou, J.; Aprea, P.; Deng, H. X. Amino-functionalized ceria with enhanced daylight photocatalytic efficiency. *Ceram. Int.* **2016**, 42, 7440-7446.

[21] Yan, X.; Zhang, L.; Zhang, Y.; Yang, G.; Yan, Z. Amine-modified SBA-15: effect of pore structure on the performance for CO_2 capture. *Ind. Eng. Chem. Res.* **2011**, 50, 3220-3226.

[22] Deng, S.; Liu, H.; Zhou, W.; Huang, J.; Yu, G. Mn-Ce oxide as a high-capacity adsorbent for fluoride removal from water. *J. Hazard. Mater.* 2011, 186, 1360-1366.

[23] Zhang, G.; He, Z.; Xu, W.; A low-cost and high efficient zirconium-modified-Na-attapulgite adsorbent for fluoride removal from aqueous solutions. *Chem. Eng. J.* **2012**, 183, 315-324.

[24] Ahmed, A. A. A.; Talib, Z. A.; Hussein, M. Z. B. Thermal, optical and dielectric properties of Zn-Al layered double hydroxide. *Appl. Clay Sci.* **2012**, 56, 68-76.

[25] Mei, Y.; Wang, W.; Nie, Z. R. Influence of pH on morphology and formation mechanism of CeO_2 nanocrystalline. *J. Rare Earth* **2007**, 25, 53-57.

[26] Pua, Z. Y.; Zhou, H.; Zheng, Y. F.; Huang, W. Z.; Li, X. N. Enhanced methane combustion over Co_3O_4 catalysts prepared by a facile precipitation method: effect of aging time. *Appl. Surf. Sci.* **2017**, 410, 14-21.

[27] Kim, J.; Desch, R. J.; Thiel, S. W.; Guliants, V. V.; Pinto, N. G. Adsorption of biomolecules on mesostructured cellular foam silica: effect of acid concentration and aging time in synthesis. *Microporous Mesoporous Mater.* **2012**, 149, 60-68.

[28] Palacios, E.; Leret, P.; Mata, M. J.; Fernandez, J. F.; Aza, A. H. D.; Rodrguez, M. A. Influence of the pH and ageing time on the acid aluminum phosphate synthesized by precipitation. *CrystEngComm* **2013**, 15, 3359-3365.

[29] Balasubramanian, M.; Melendres, C. A.; Mansour, A. N. An X-ray absorption study of the local structure of cerium in electrochemically deposited thin films. *Thin Solid Films* **1999**,

347, 178-183.

[30] Liu, X.; Zhou, L.; Fu, X.; Sun, Y.; Su, W.; Zhou, Y. Adsorption and regeneration study of the mesoporous adsorbent SBA-15 adapted to the capture/separation of CO_2 and CH_4. *Chem. Eng. Sci.* **2007**, 62, 1101-1110.

[31] Wu, X.; Zhang, Y.; Dou, X.; Zhao, B.; Yang, M. Fluoride adsorption on an Fe-Al-Ce trimetal hydrous oxide: characterization of adsorption sites and adsorbed fluorine complex species. *Chem. Eng. J.* **2013**, 223, 364-370.

[32] Dimos, K.; Stathi, P.; Karakassides, M. A.; Deligiannakis, Y. Synthesis and characterization of hybrid MCM-41 materials for heavy metal adsorption. *Microporous Mesoporous Mater.* **2009**, 126, 65-71.

[33] Vardikara, H. S.; Bhanvasea, B. A.; Rathodb, A. P.; Sonawane S. H. Sonochemical synthesis, characterization and sorption study of Kaolin-Chitosan-TiO_2 ternary nanocomposite: Advantage over conventional method. *Mater. Chem. Phys.* 2018, 217: 457-467.

[34] Ahmed, S. M.; El-Dib, F. I.; El-Gendy, N. S.; Sayed, W. M.; EI-Khodary, M. A kinetic study for the removal of anionic sulphonated dye from aqueous solution using nano-polyaniline and Baker's yeast. *Arab. J. Chem.* **2012**, 28, 358-367.

[35] Mahmoodi, N. M.; Bagherpour, F.; Nariyan, E. Amine functionalized magnetic carbon nanotube: synthesis and binary system dye removal. *Desalin. Water Treat.* **2015**, 56, 107-120.

[36] Mahmoodi, N. M.; Najafi, F. Synthesis, amine functionalization and dye removal ability of titania/silica nano-hybrid. *Microporous Mesoporous Mater.* **2012**, 156, 153-160.

[37] Gao, J. F.; Wang, J. H.; Yang, C.; Wang, S. Y.; Peng, Y. Z. Binary biosorption of Acid Red 14 and Reactive Red 15 onto acid treated okara: simultaneous spectrophotometric determination of two dyes using partial least squares regression. *Chem. Eng. J.* **2011**, 171, 967-975.

[38] Wei, A.; Liu, B.; Zhao, H.; Chen, Y.; wang, W. Synthesis and formation mechanism of flowerlike architectures assembled from ultrathin NiO nanoflakes and their adsorption to malachite green and acid red in water. *Chem. Eng. J.* **2014**, 239, 141-148.

[39] Khodam, F.; Rezvani, Z.; Amani-Ghadim, A. R. Enhanced adsorption of Acid Red 14 by co-assembled LDH/MWCNTs nanohybrid: optimization, kinetic and isotherm. *J. Ind. Eng. Chem.* **2015**, 21, 1286-1294.

[40] He, L.; Li, J.; Feng, Z.; Sun, D.; Wang, T.; Li, R.; Xu, Y. Solvothermal synthesis and characteriazation of ceria with solid and hollow spherical and multilayered morphologies. *Appl. Surf. Sci.* **2014**, 322, 147-154.

[41] Ji, P.; Zhang, J.; Chen, F.; Anpo, M. Study of adsorption and degradation of acid orange 7 on the surface of CeO_2 under visible light irradiation. *Appl. Catal. B: Environ.* **2009**, 85, 148-154.

ACCEPTED MANUSCRIPT

Figure captions

Fig. 1 Effect of reaction temperature on the removal of 250 mg/l AR14 at room temperature and pH of 5.32 ($CeO_2 \cdot xH_2O$ was synthesized at pH of 9.5 and aged for 6 h, $m_{CeO2 \cdot xH2O}$=0.02 g, V_{AR14}=20 ml).

Fig. 2 In situ FT-IR spectra of samples synthesized at different temperatures after evacuation under vacuum for 4 h: (a) 25 ^{O}C, (b) 40 ^{O}C, (c) 55 ^{O}C.

Fig. 3 Effect of reaction pH on the removal of 250 mg/g AR14 at room temperature and pH of 5.32 ($CeO_2 \cdot xH_2O$ was synthesized at 25 ^{O}C and aged for 6 h, $m_{CeO2 \cdot xH2O}$=0.02 g, V_{AR14}=20 ml).

Fig. 4 FT-IR spectra of $CeO_2 \cdot xH_2O$ prepared at different pH value (reaction temperature: 25 ^{O}C, aging time: 12 h) (a) and $CeO_2 \cdot xH_2O$ prepared at pH of 8.5 before and after adsorption of AR14 (b).

Fig. 5 Effect of precipitant on the removal of 250 mg/g AR14 at room temperature and pH of 5.32 ($CeO_2 \cdot xH_2O$ was synthesized at 25 ^{O}C and aged for 6 h, $m_{CeO2 \cdot xH2O}$=0.02 g, V_{AR14}=20 ml).

Fig. 6 Effect of aging time on the removal of 250 mg/l AR14 at room temperature and pH of 5.32 ($CeO_2 \cdot xH_2O$ was synthesized at 25 ^{O}C and pH of 9.5, $m_{CeO2 \cdot xH2O}$=0.02 g, V_{AR14}=20 ml).

Fig. 7 FT-IR spectra of $CeO_2 \cdot xH_2O$ prepared at different aging time (reaction temperature: 25 ^{O}C, reaction pH: 8.5).

Fig. 8 XRD patterns of the target $CeO_2 \cdot xH_2O$ (a) and standard CeO_2 (b).

Fig. 9 TG and DTA profiles of the target $CeO_2 \cdot xH_2O$.

Fig. 10 XPS spectra of Ce3d (a) and O1s (b) for the target $CeO_2 \cdot xH_2O$.

Fig. 11 Removal efficiency of AR14 on the target $CeO_2 \cdot xH_2O$ at room temperature as a function of the initial pH value in 250 mg/l AR14 solution ($m_{CeO2 \cdot xH2O}$=0.02 g, V_{AR14}=40 ml).

Fig. 12 Uptake of AR14 on the target $CeO_2 \cdot xH_2O$ at room temperature and an initial pH value of 4.5 in 250 mg/l AR14 solution ($m_{CeO2 \cdot xH2O}$=0.02 g, V_{AR14}=40 ml) (a) and pseudo second order kinetics model correlation (b).

Fig. 13 Adsorption isotherm of AR14 on the target $CeO_2 \cdot xH_2O$ at room temperature and an initial pH value of 4.5 in AR14 solution. The symbols are the experimental data and the line is the Langmuir model correlations. ($m_{CeO2 \cdot xH2O}$=0.02 g, V_{AR14}=40 ml)

Fig. 14 Proposed adsorption mechanism over the target $CeO_2 \cdot xH_2O$ ($V_O^{\bullet\bullet}$: oxygen vacancy, $R\text{-}SO_3^- {}^+Na$: acid dyes such as AR14 and AO7).

ACCEPTED MANUSCRIPT

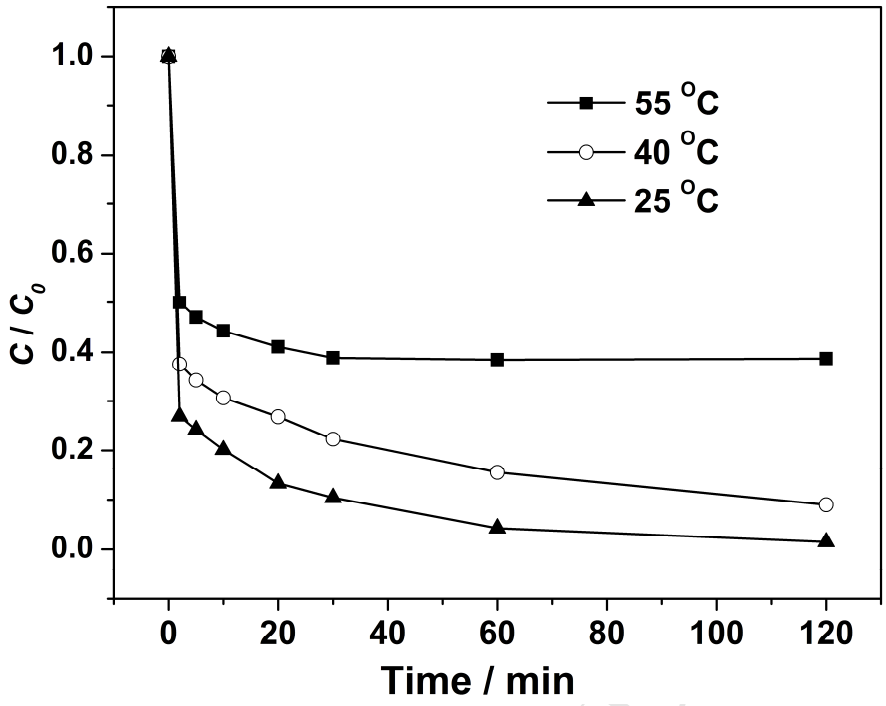
1.0
0.8
0.6
0.4
0.2
0.0
C / C0
55 °C
40 °C
25 °C
0
20
40
60
80
100
120
Time / min

Fig. 1

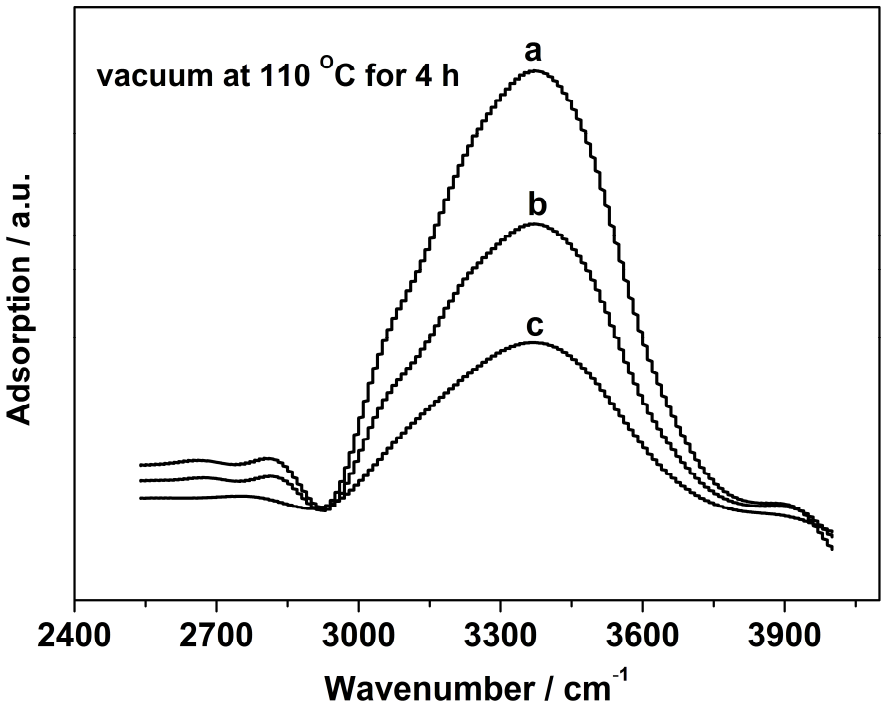
vacuum at 110 °C for 4 h
a
b
c
Adsorption / a.u.
2400
2700
3000
3300
3600
3900
Wavenumber / cm-1

Fig. 2

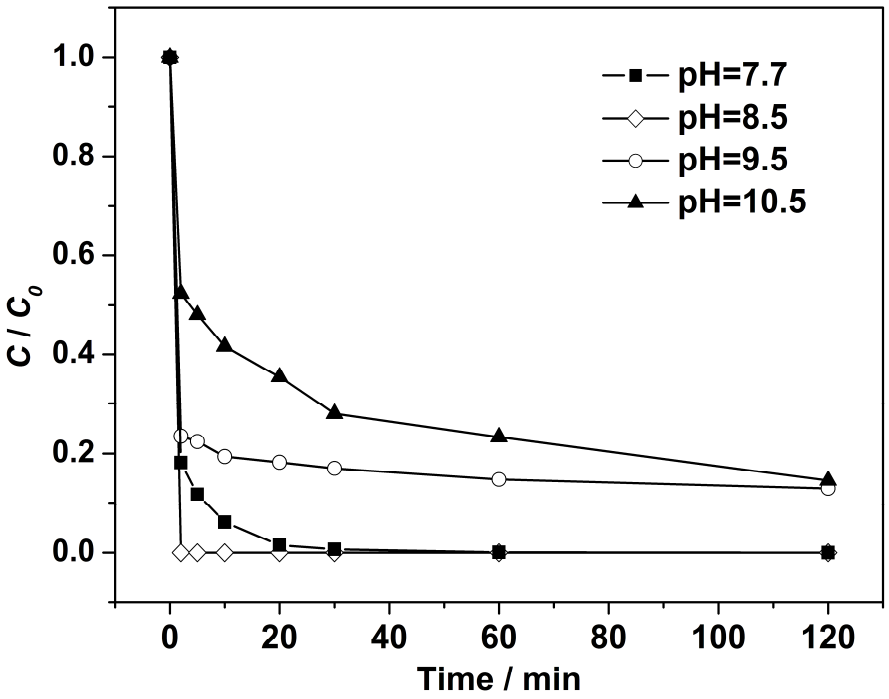
pH=7.7
pH=8.5
pH=9.5
pH=10.5
C / C0
Time / min
1.0
0.8
0.6
0.4
0.2
0.0
0
20
40
60
80
100
120

Fig. 3

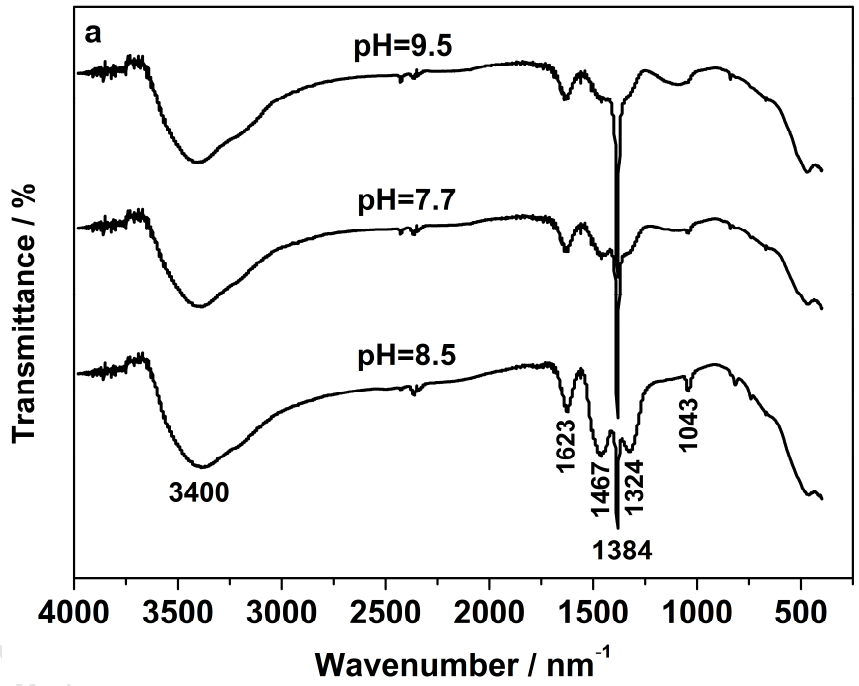
a
pH=9.5
pH=7.7
pH=8.5
Transmittance / %
3400
1623
1467
1384
1324
1043
4000
3500
3000
2500
2000
1500
1000
500
Wavenumber / nm-1

Fig. 4a

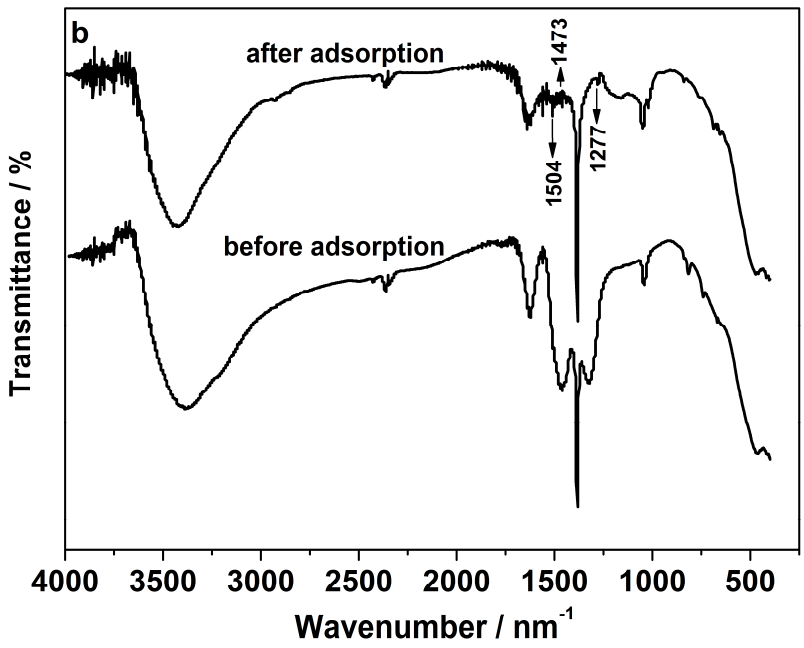
b
after adsorption
before adsorption
1473
1504
1277
Transmittance / %
4000
3500
3000
2500
2000
1500
1000
500
Wavenumber / nm-1

Fig. 4b

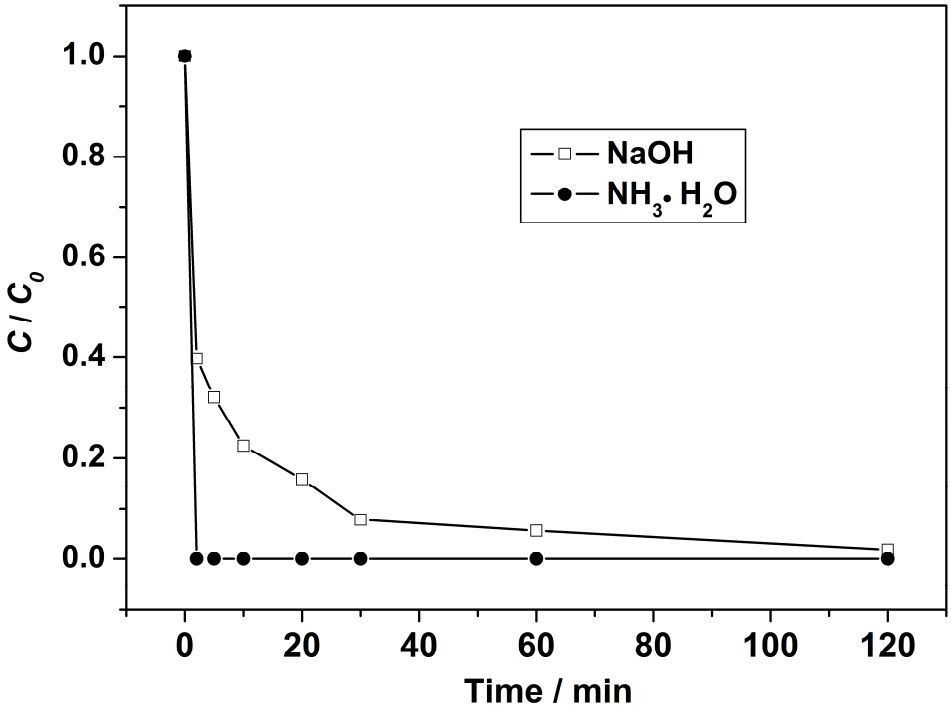
NaOH
NH3• H2O
C / C0
1.0
0.8
0.6
0.4
0.2
0.0
0
20
40
60
80
100
120
Time / min

Fig. 5

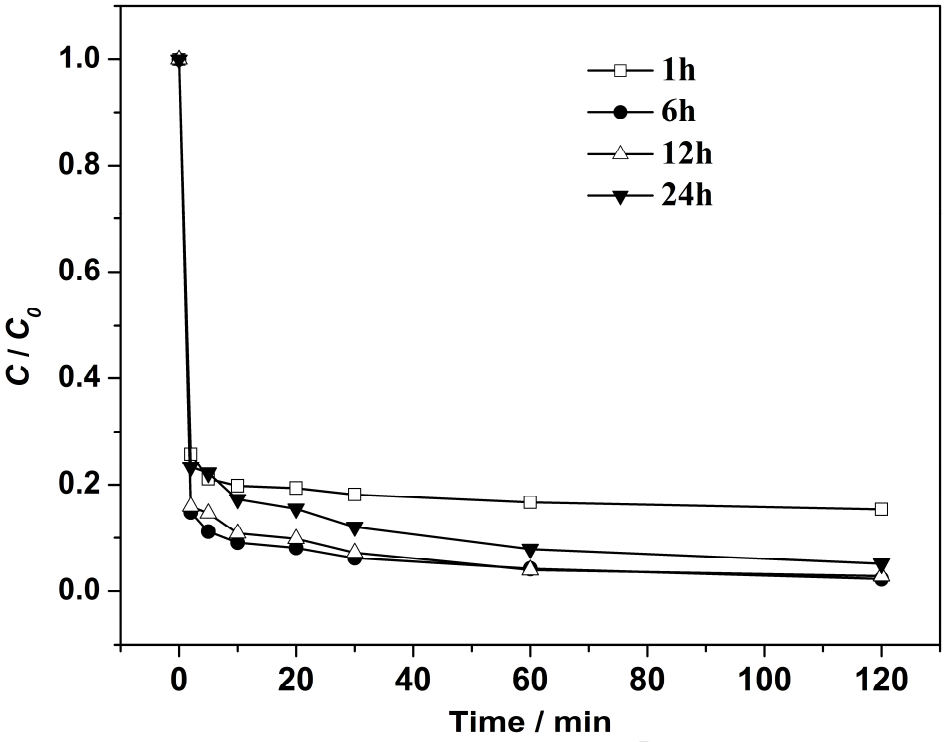
1.0
0.8
0.6
0.4
0.2
0.0
C / C0
0
20
40
60
80
100
120
Time / min
1h
6h
12h
24h

Fig. 6

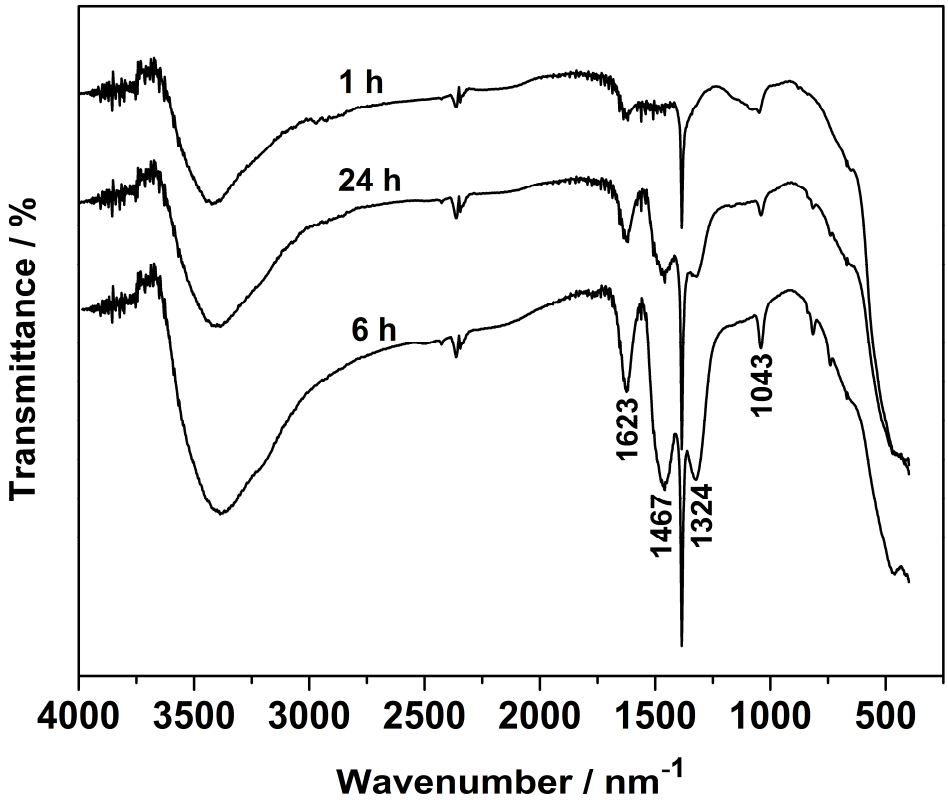
Transmittance / %
1 h
24 h
6 h
1623
1467
1324
1043
4000
3500
3000
2500
2000
1500
1000
500
Wavenumber / nm-1

Fig. 7

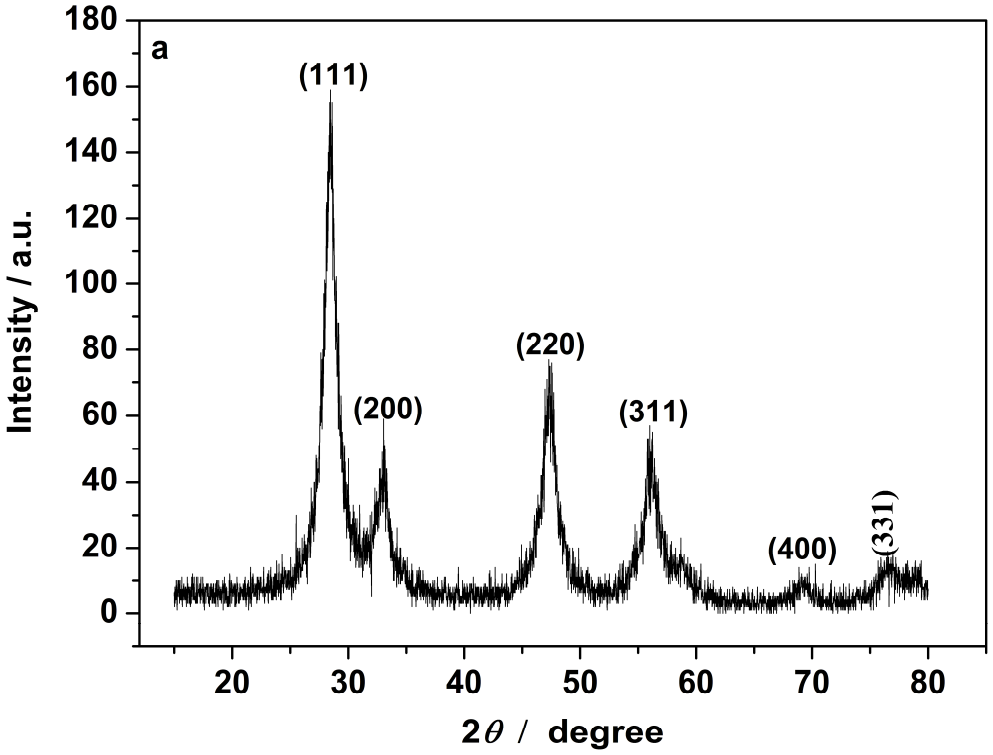
a
(111)
(200)
(220)
(311)
(400)
(331)
Intensity / a.u.
2θ / degree

Fig. 8a

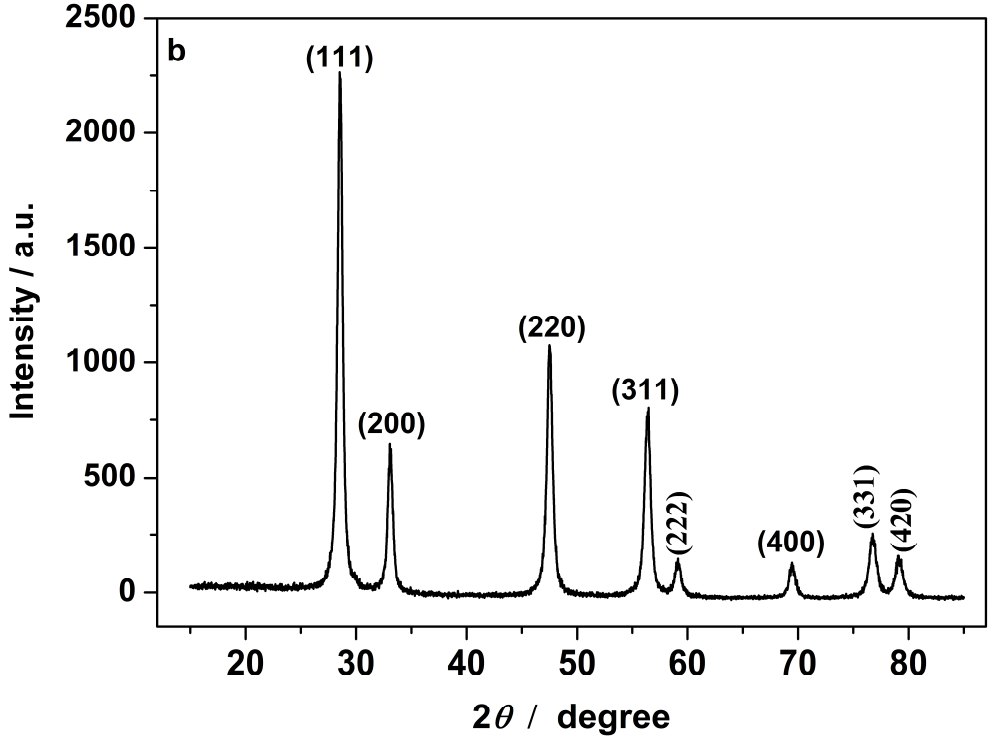
b
(111)
(200)
(220)
(311)
(222)
(400)
(331)
(420)
Intensity / a.u.
2θ / degree

Fig. 8b

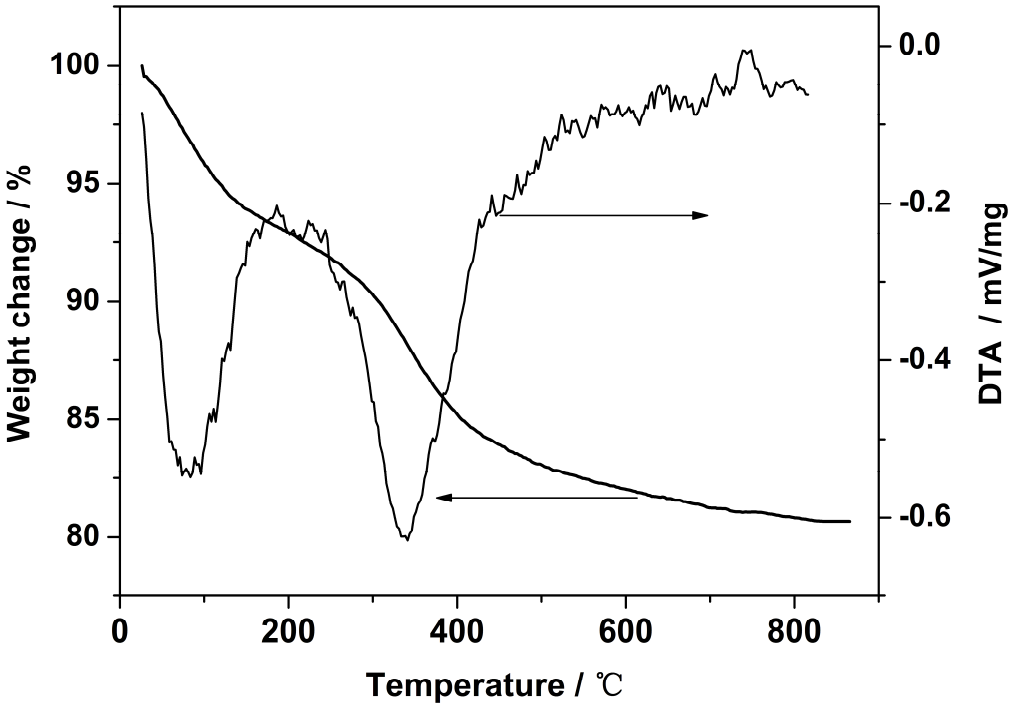
Weight change / %
100
95
90
85
80
0.0
-0.2
-0.4
-0.6
DTA / mV/mg
0
200
400
600
800
Temperature / ℃

Fig. 9

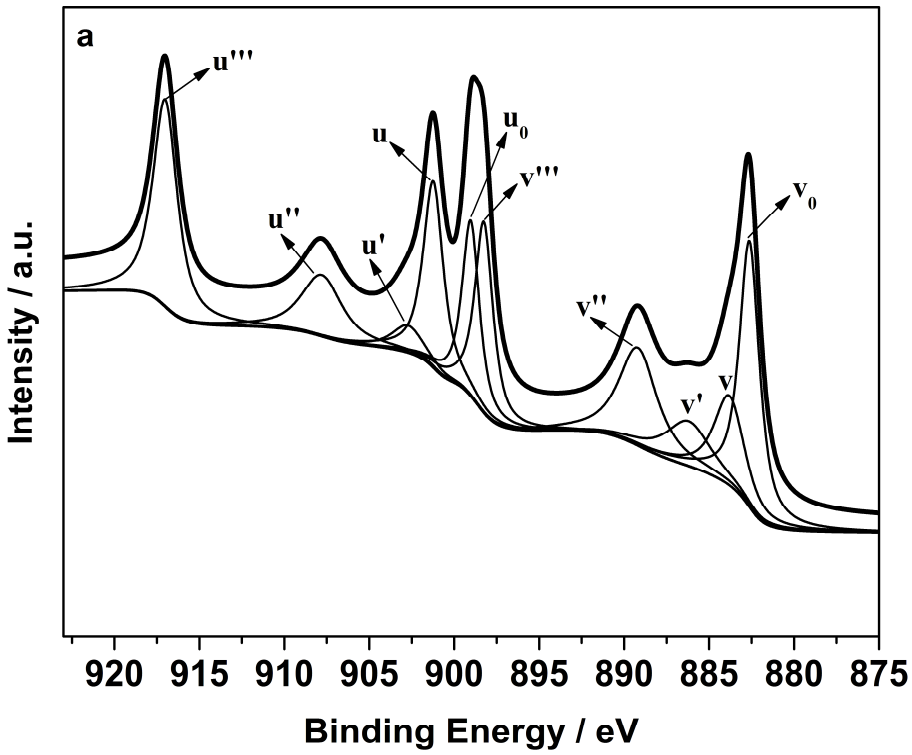
a
u'''
u
u0
v'''
u''
u'
v0
v''
v
v'
Intensity / a.u.
920
915
910
905
900
895
890
885
880
875
Binding Energy / eV

Fig. 10a

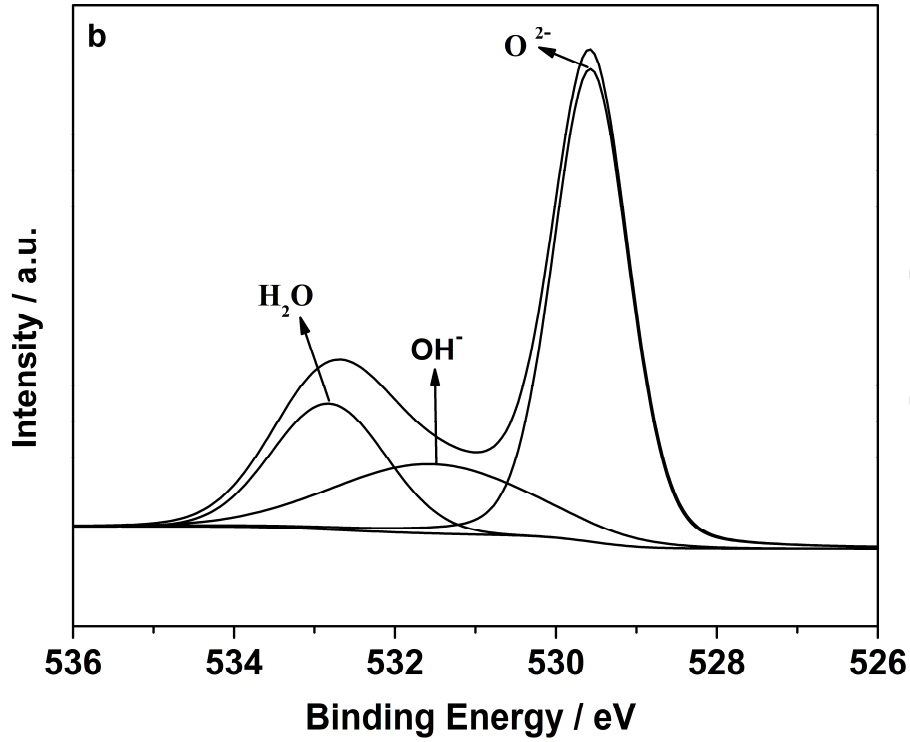

Fig. 10b

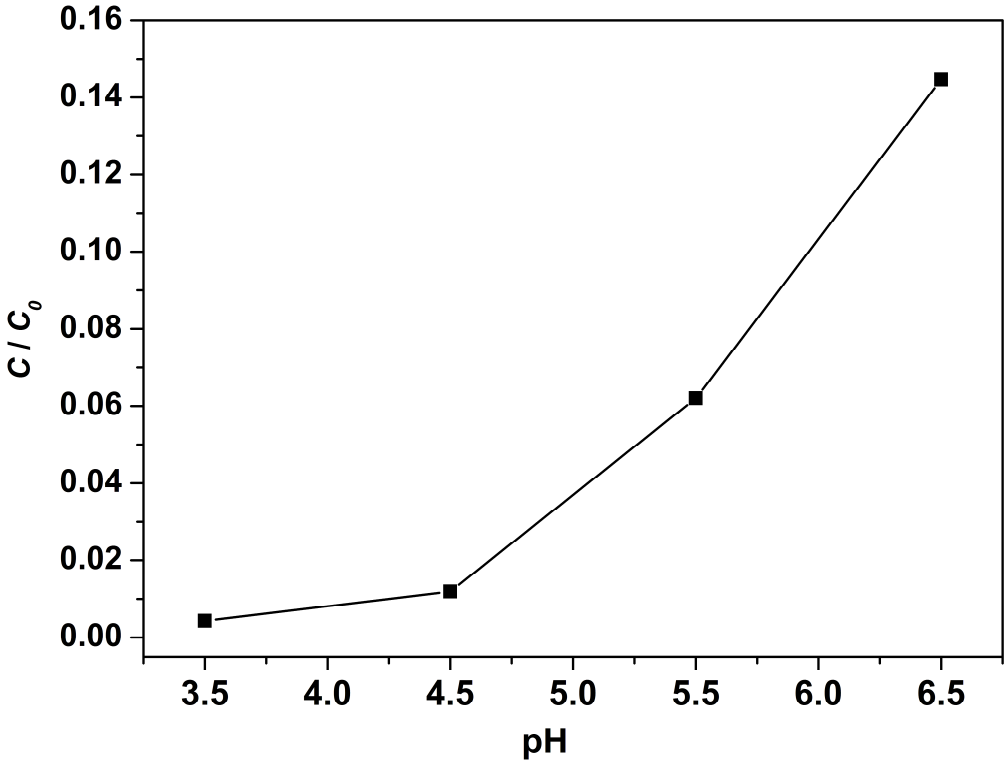

Fig. 11

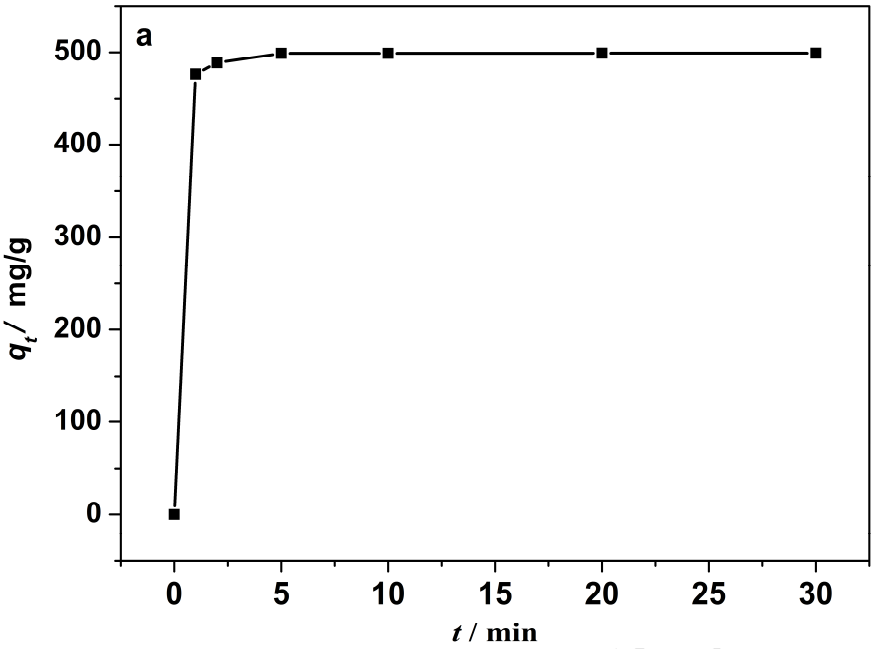

Fig. 12a

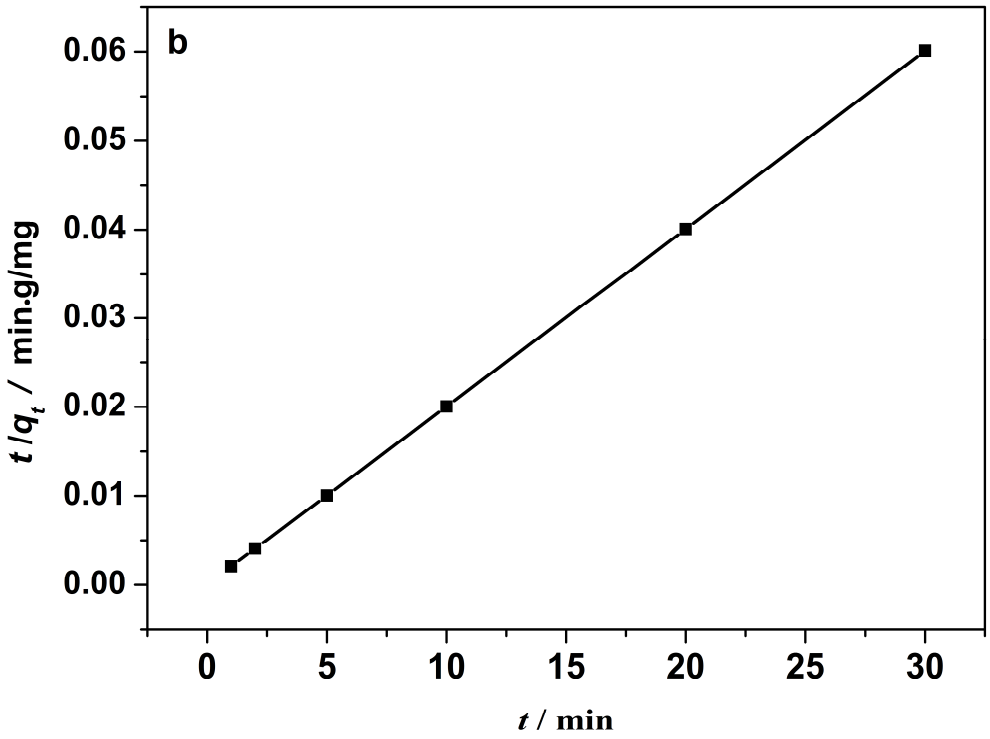

Fig. 12b

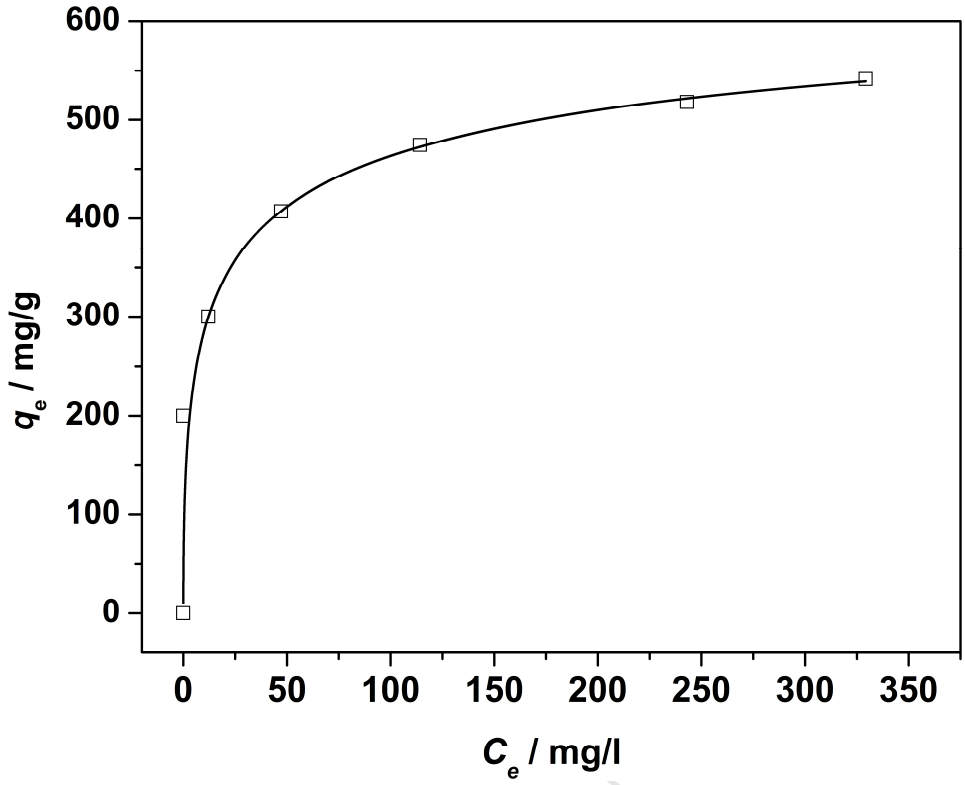
600
500
400
300
200
100
0
q_e / mg/g
0
50
100
150
200
250
300
350
C_e / mg/l

Fig. 13

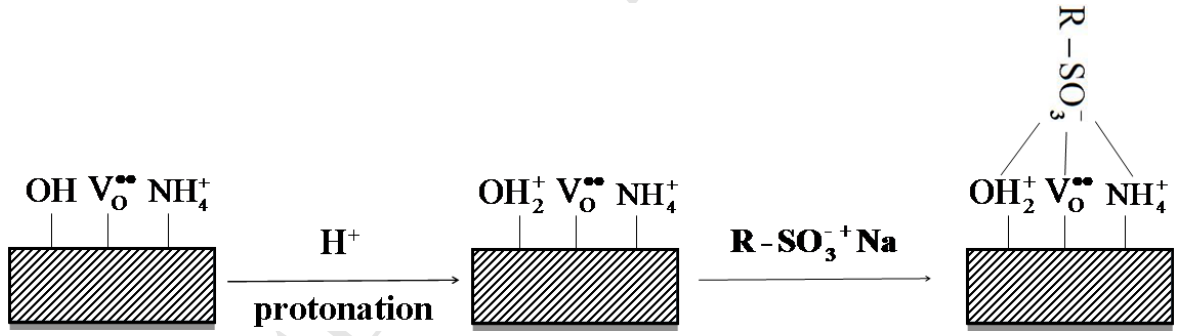
OH $V_O^{\bullet\bullet}$ NH_4^+
H^+
protonation
OH_2^+ $V_O^{\bullet\bullet}$ NH_4^+
$R-SO_3^-{}^+Na$
$R-SO_3^-$
OH_2^+ $V_O^{\bullet\bullet}$ NH_4^+

Fig. 14

ACCEPTED MANUSCRIPT

Highlights

- $CeO_2 \cdot xH_2O$ with high loading of hydroxyl groups was synthesized *via* a facile method.
- Numerous ammonium radicals and oxygen vacancies were detected in $CeO_2 \cdot xH_2O$.
- Acid red 14 and acid orange 7 were efficiently removed by $CeO_2 \cdot xH_2O$.
- A novel adsorption mechanism was proposed.
- A practical application of the optimized $CeO_2 \cdot xH_2O$ was expected.

ACCEPTED MANUSCRIPT